Characterization and modeling of tropospheric propagation at high latitudes for satcom systems

Luc Frison, Julien Queyrel, Laurent Feral

Characterization and modeling of tropospheric propagation at high latitudes for satcom systems

Luc Frison ONERA/DEMR, Université de Toulouse, F-31055 Toulouse, France,
luc.frison@onera.fr
Julien Queyrel, ONERA/DEMR, Université de Toulouse, F-31055 Toulouse, France,
julien.queyrel@onera.fr
Laurent Feral, Laboratoire d'aérologie, Université Toulouse 3, France
laurent.feral@aero.obs-mip.fr

Abstract

The work presented in this paper aims at developing and evaluating the potentialities of a high-resolution meteorological model coupled with an electromagnetic module to produce reliable tropospheric attenuation statistics at polar latitudes. To do so, an Atmospheric Numerical Simulator (ANS) based on the high-resolution weather model PWRF-ARW dedicated to polar latitudes is used to generate 3D daily states of the atmosphere in Svalbard (Norway, 80° north latitude) at high spatial (2×2km²) and temporal (5mn) resolutions. Because of considerable computational times, this preliminary work focuses on the simulation of a single day (2017/02/21) during which typical polar precipitations occur. First, the PWRF meteorological outputs relevant for propagation purposes (3D atmospheric datacubes) are compared with reference reanalysis data (Arome-Arctic, CARRA, ERA5) as well as meteorological measurements collected during the THOR7 propagation experiment based on the Svalbard archipelago. Second, an electromagnetic module is used to convert the PWRF meteorological output datacubes into tropospheric attenuation time series simulating the link at Ka band between the THOR7 beacon and the SvalSat teleport. These are compared with the experimental time series collected during the THOR7 propagation experiment. Synthetic attenuation statistics are also produced for that specific day and compared to the experimental statistics derived from the THOR7 propagation experiment. On the 2017/02/21, the results show a good agreement between PWRF outputs and the other meteorological data sources. Additionally, if the synthetic attenuation times series reproduces quite well the experimental time series dynamics, the statistical analysis reveals overestimations that could be explained by either an approximative modeling of the hydrometeors in mixed-phase or wrong predicted hydrometeors contents.

1. Introduction

Due to global warming, the polar regions are increasingly accessible and offer new opportunities that require the deployment of terrestrial or space telecommunications systems. For example, Earth observation satellites in polar orbit could take advantage of their increased daily visibility to transfer data to high latitudes ground stations more often; ships using the new maritime routes also need access to Satcom services provided by satellites in geostationary orbit. However, at these latitudes, the radio links are established at very low elevation angles (a few degrees at most). Consequently, the associated radioelectric paths through the troposphere are considerably increased, which intensifies the propagation effects (attenuation, refraction, scintillation) classically observed at lower latitudes. On the other hand, in order to reach high data rates, the satcom systems considered must operate beyond 20 GHz. However, at these frequency bands, the total tropospheric attenuation due to oxygen, water vapor, clouds and hydrometeors in liquid phase (rain) or mixed phase (wet snow) can become prohibitive [1]. To these attenuations are added small scale turbulent fluctuations of the tropospheric refractive index. They are responsible for scintillation effects that become very significant for such low elevation links. Finally, at larger scales, specific refraction effects (surface or altitude duct) are likely to appear along these extended slant paths.

In order to quantify these propagation effects for the optimal design of polar Telecom systems, empirical propagation models are usually derived from experimental campaigns. Unfortunately, such propagation experiments are costly and difficult to maintain in Polar Regions. Following [1], [2] or [3],

our approach consists in modeling the various tropospheric propagation effects by coupling a high-resolution meteorological model, PWRF-ARW (Polar WRF [4], polar version of the Advanced Research Weather Research and Forecasting WRF-ARW model [5]) to an ElectroMagnetic Module (EMM). The set PWRF-EMM defines the Atmospheric Numerical Simulator ANS which is presented in Section 2. Its performances will be evaluated on a single day by comparing with meteorological and propagation data, presented in Section 3. Finally, the results are given in Section 4.

2. The Atmospheric Numerical Simulator (ANS)

The PWRF-ARW model is used to produce a 3D description of the atmosphere every 5 min over an area of about 200×200 km² (horizontal resolution 2×2km²) centered halfway through the ground projection of the SvalSat (78.25°N, 15.50°E) – THOR7 tropospheric slant path. The outputs are sampled over 38 vertical model levels (ranging from ground level to ~20km). The ERA5 re-analysis data (§3) are used for the initial and boundary conditions of the simulation. In order to mimic realistic past states of atmosphere, the simulations length is limited to one day with an initialization period of 12 hours (the results of which are later discarded) allowing the model to provide stable outputs. In compliance with Figure 1, to reach the final resolution of 2x2km², two nested domains are used: a coarser domain d01 (horizontal resolution of 10x10km² constructed with a polar stereographic projection and static fields initialized directly by interpolation from the ERA5 database), finer domain d02 nested at the center of the former, at the desired resolution (2x2km²). Each output 3D voxel of a datacube provides information on several meteorological variables (temperature T, pressure P, humidity H, concentration of precipitating hydrometeors, etc.) which depend on an exhaustive parametrisation, part of which is the microphysical scheme (interaction models between the various water phases). In our case, a cumulus scheme is activated for the large domain d01 only (Tiedtke diagram [6]). To reduce the computational time, d01 is hydrostatic and d02 non-hydrostatic (defining d01 as a non-hydrostatic domain is time-consuming but does not change the simulation results significantly). The spectral nudging model provided within PWRF is also used in order to generate realistic simulations when compared to the ERA5 reanalysis data.

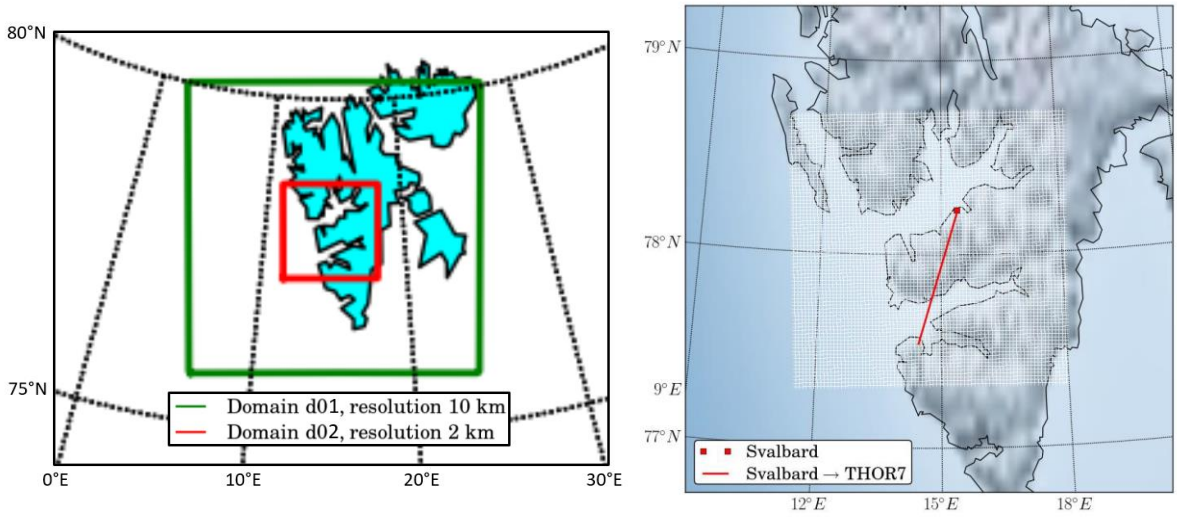

Figure 1: The two nested d01 end d02 domains of the PWRF-ARW simulations (a) and position of the high-resolution domains d02 with the horizontal projection of the line of sight towards the THOR7 satellite (b)

An ElectroMagnetic Module (EMM) written in Python then converts the atmospheric parameters of interest (pressure P, temperature T, water vapor content ρ_{vap}, cloud water content ρ_{cloud}, rain water content ρ_{rain}) within the 3D meteorological voxels simulated every 5 min by PWRF into specific attenuations (in dB/km) for each tropospheric contributor to the total attenuation: oxygen, water vapor, cloud, rain and snow. The integration of the specific attenuation along the line of sight towards THOR7 allows to recover the attenuation suffered by the signal through the troposphere.

The physical models used by the EMM are: the line-by-line spectral model of recommendation ITU-R P676-11 for oxygen and water vapor and the model based on Rayleigh scattering of ITU-R P840 -7 for cloud droplets.

The granulometry of the precipitating hydrometeors (rain, dry and wet snow) is estimated from the content (g/m3) and the number of particules given by PWRF in each voxel. Here, the Thompson microphysical scheme [7] is used because it is well suited for high latitudes simulations, providing information on several types of polar hydrometeors such as snow, ice and graupel in addition to rain. The granulometry of each water phase component x is then given by:

$$N_x(D_x) = N_{Tx}\frac{1}{\Gamma(1+\alpha_x)}\left[\frac{N_{Tx}M_{sx}\pi}{6\rho_x}\frac{\Gamma(4+\alpha_x)}{\Gamma(1+\alpha_x)}\right]^{\frac{1+\alpha_x}{3}} e^{-\left[\frac{N_{Tx}M_{sx}\pi}{6\rho_x}\frac{\Gamma(4+\alpha_x)}{\Gamma(1+\alpha_x)}\right]^{\frac{1}{3}}D_x} \quad (1)$$

With x ∈ [snow, rain, ice, graupel], N_x the number of hydrometeors with diameter D_x per unit volume, α_x= 0 [4], M_{sx} the density of the hydrometeor x, Γ the gamma function, ρ_x the mixing ratio and N_{Tx} the concentration of component x. Importantly, note that ρ_x and N_{Tx} are PWRF outputs.

The phase of the hydrometeors (rain, ice, dry snow, wet snow) is also taken into account by using the Sihvola equivalent permittivity model [8]. It makes it possible to determine the equivalent permittivity of a mixed hydrometeor as a function of the mass fractions composing it. The single-phase permittivity is computed from the double Debye model [9]. Then, the associated specific attenuation γ_x is calculated using the theory of scattering by spherical (Mie formulation for rain) or spheroidal (T-matrix formulation for dry and wet snow) scatterers for which the axis ratio is a function of the size and type of hydrometeor.

$$\gamma_x = 4.343 \times 10^3 \int_0^{D_{max}} \sigma_{ext}(D)N(D)dD \quad (2)$$

With $\boldsymbol{\sigma_{ext}(D)}$ the extinction cross section derived from Mie theory or from the Tmatrix for respectively x=rain or x=snow, $\mathbf{D_{max}}$ is the maximum diameter of a hydrometeor of category x. $\mathbf{D_{max}}$ = 6mm for rain and $\mathbf{D_{max}}$ = 8mm for snow [10].

Following the approach proposed for rain in [11] and considering the limit values of axis ratio found by Garret [12] in measurement - $a = 0.45$ for $D_{e,max}$ = 8mm [10], the following relation for the axis ratio for snow has been adopted:

$$a(D_e) = 0.9643 - 0.0643 * D_e \quad 0 < D_e < 8mm$$

With $\mathbf{D_e}$, the equivalent diameter of water content

In order to calculate the total attenuation suffered by the signal along its path towards the beacon receiver at low elevation angles, large-scale geometric refraction effects are also taken into account. First, for each time step, a vertical slice of atmosphere, directed towards the satellite is extracted from the PWRF data cube. Next, a dichotomy algorithm is used to estimate the true elevation angle of the geometric path between the beacon receiver and the satellite by propagating a geometric ray through the different layers of atmosphere within the slice. The refractive index (computed from P, T and $\boldsymbol{\rho_{vap}}$ with Rec. ITU-R P.453-13) is used to apply the geometric laws of Snell/Descartes between two successive layers as suggested in ITU-R P.676-11. In order to propagate the signal to THOR7, starting at SvalSat the process is repeated for different elevation angles until the beacon receiver and satellite are joined within an acceptable margin of error. The specific attenuation is then integrated along the newly found geometric path to recover the total attenuation (dB) at the current time step.

3. Experimental and re-analysis database for validation.

In order to assess the performance of the ANS, various datasets are used as a basis for comparison.

3.1 ERA5 [13]
Although used as initial and boundary conditions in PWRF, the ERA5 reanalysis data produced by the European Center for Weather Prediction (ECMWF) are also considered to evaluate the weather outputs produced by our model. ERA5 data provide an hourly estimate of various meteorological quantities (temperature, pressure, cumulative precipitation, etc.) at any point on the globe with a horizontal resolution of 0.25x0.25deg² on 38 vertical pressure levels as well as single level and surface quantities.

3.2 Arome Arcitc [14]
PWRF simulations will be compared with Arome-Arctic reanalysis provided by the Norwegian Meteorological Institute. These reanalysis data come from the Arome meteorological model developed by Meteo-France centered on the Arctic zone (horizontal resolution 2.5×2.5km², 65 vertical pressure levels).

3.3 CARRA [15]
The simulations will also be compared with the Copernicus Arctic Regional Reanalysis (CARRA) dataset. It contains 3-hour analyses and short-term hourly forecasts of atmospheric and surface weather variables such as temperature and humidity (but no rainfall data) at 2.5x2.5km² resolution over 23 vertical pressure levels.

3.4 THOR7 experiment (WX) [16]
In order to study the specificities of the Ka-band propagation channel at polar latitudes, ESA financed a two-year campaign (April 2016 to March 2018) of propagation at 20 GHz between the geostationary satellite THOR-7 and a NASA beacon receiver installed at the Svalbard Satellite Teleport (SvalSat) operated by KSAT on the island of Spitsbergen in the Svalbard archipelago of Norway. With the help of NASA and additional funding from CNES, ONERA was in charge of analyzing the propagation data [1]. The experimental ground station consists in a beacon receiver designed by the NASA Glenn Research Centre [16] that operates in the Ka-band at the 20.198 GHz beacon frequency of THOR7which is seen with a 2.65° elevation angle from SvalSat. A Ka-band radiometer (Radiometric PR-2230) that can observe multiple channels between 22 and 30 GHz is also available on site. Other meteorological instruments such as tipping bucket rain gauge and a weather station equipped with an IR cloud sensor complement the equipment deployed for this experiment (see Figure 2). During the measurement campaign, it was noted that meteorological conditions (precipitation and low temperature) could interfere with the proper functioning of the tipping bucket (freezing problems) and generate faulty measurements.

Figure 2 : SvalSat station (78.25°N, 15.50°E)

4. ANS simulator validations

Due to the large computation time of the PWRF simulations, we focus in this study on a single daily simulation. The 2017-02-21 was selected by searching for a snowy day with attenuation events within the precipitation and temperature data from Arome-Arctic and in the in-excess attenuation time series obtained by plotting THOR7 data completed with the concurrent WX meteorological measurements collected at the SvalSat station (temperature during the day always below 273K and precipitation measurement).

4.1 Meteorological outputs

In order to verify the ability of our model to reproduce the states of the polar atmosphere, we will first focus on meteorological variables from PWRF simulations. In particular, the evolution of temperature and humidity during the 2017-02-21 at the coordinates of the SvalSat station (latitude: 78.22, longitude: 15.42, height: 465m) are shown in Figures 3 and 4 respectively. Note that the reference data and the simulated data do not have the same temporal and spatial sampling: Table 1 summarizes the differences.

	ERA	CARRA	Arome-Arctic	Wx	PWRF
Pressure Levels (PL)	38 vertical model levels	23 vertical model levels	65 vertical model levels	/	38 vertical model levels
Temperature and humidity	4D data, 0.25°x0.25°x 38 x 1h	4D data, 2.5x2.5km² x 23 x 3h	4D data, 2.5x2.5 km² x 65 x 1h	time series at SvalSat (10Hz)	4D data, 2x2 km² x 38 x 5mins
Precipitation accumulation	3D data, average over 0.25°x0.25° x1h	3D data, average over 2.5x2.5 km² x 3h	3D data, average over 2.5x2.5 km² x 1h	time series at SvalSat (10Hz)	3D data, average over 2x2 km² x 5min

Table 1 : Temporal and spatial sampling for ERA, CARRA, Arome Arctic, WX and PWRF

In Figure 3 and 4, the results of the PWRF simulations are plotted in black, those from the ERA5 reanalysis in red, in yellow those related to Arome-Arctic, and in blue the CARRA data. The meteorological data (WX temperature in Figure 3, WX humidity in Figure 4) collected at the SvalSat station during the THOR7 propagation campaign are reported in green. All simulations and reanalysis

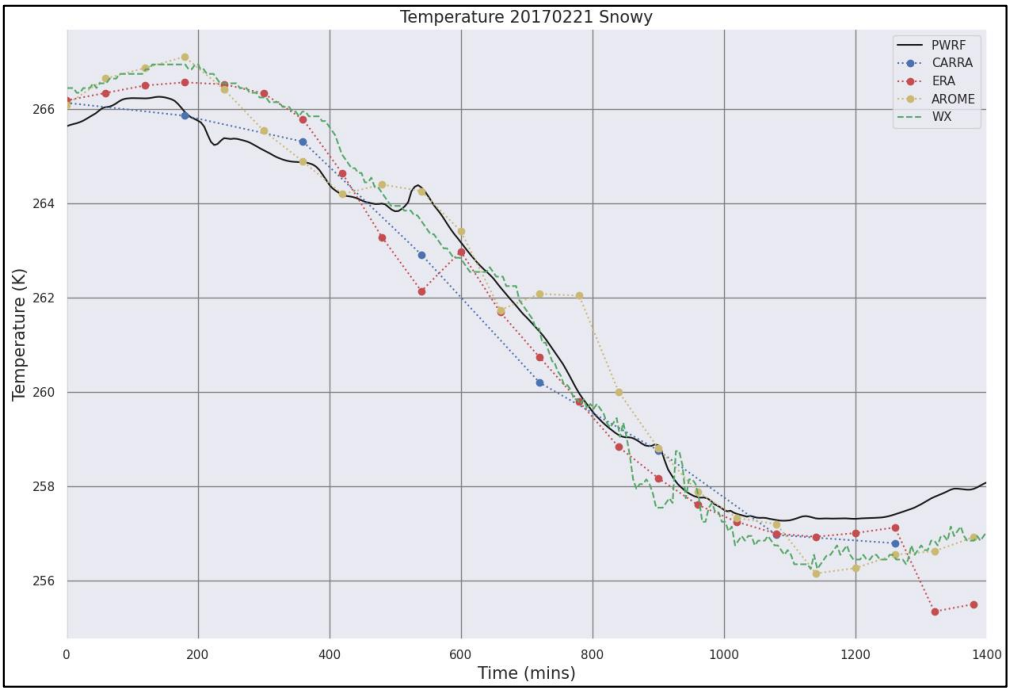

Figure 3: Temperature temporal evolution, SvalSat, 02-21-2017 from PWRF simulations and from the various reference meteorological databases.

data (PWRF, CARRA, ERA5 and Arome Arctic) are interpolated at the height of the THOR7 experimental station (465m) in order to obtain comparable curves. Figure 3 shows a good agreement between the PWRF simulations and the reanalysis or the WX weather station data: PWRF seems to produce temperature outputs consistently with the four sets of references. However, Figure 4 shows that the simulated humidity time series at the position and height of the SvalSat station are less comparable with the reanalysis or WX time series. Nevertheless, despite a specific moisty event in the first part of the day, the model seems to reproduce the experimental and reanalysis data quite faithfully.

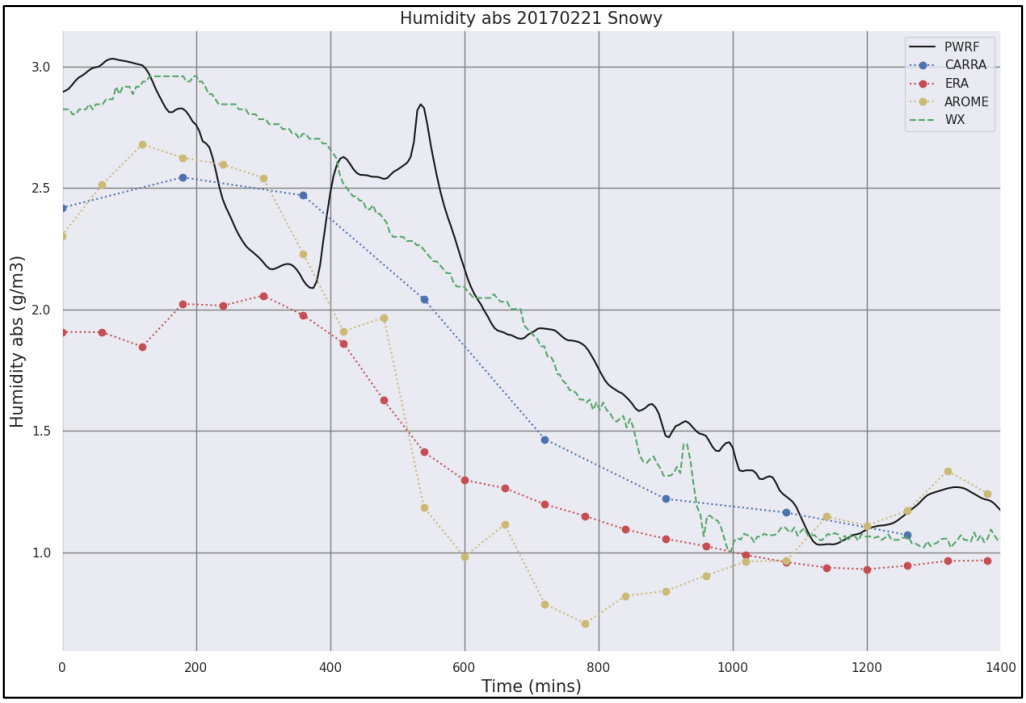

Figure 4 : Humidity temporal evolution, SvalSat, 02-21-2017 from PWRF simulations and from the various reference meteorological databases.

The next step towards the PWRF weather model validation effort focuses on its ability to reproduce accumulated precipitation contents during the whole day. The microphysical scheme selected to run PWRF in this study makes it possible to isolate four distinct types of precipitations: rain, snow, ice and graupel. We consider the amount of total precipitation as the addition of the number of millimeters of equivalent water of each kind. Figure 5 shows the time series of cumulative precipitations within the pixel centered on the SvalSat station coordinates for the 2017-02-21. The data from ERA5 are also plotted for information only (the 0.25°x0.25° horizontal resolution of ERA5 is very different from the 2x2km² horizontal resolution of Arome-Arctic and PWRF.

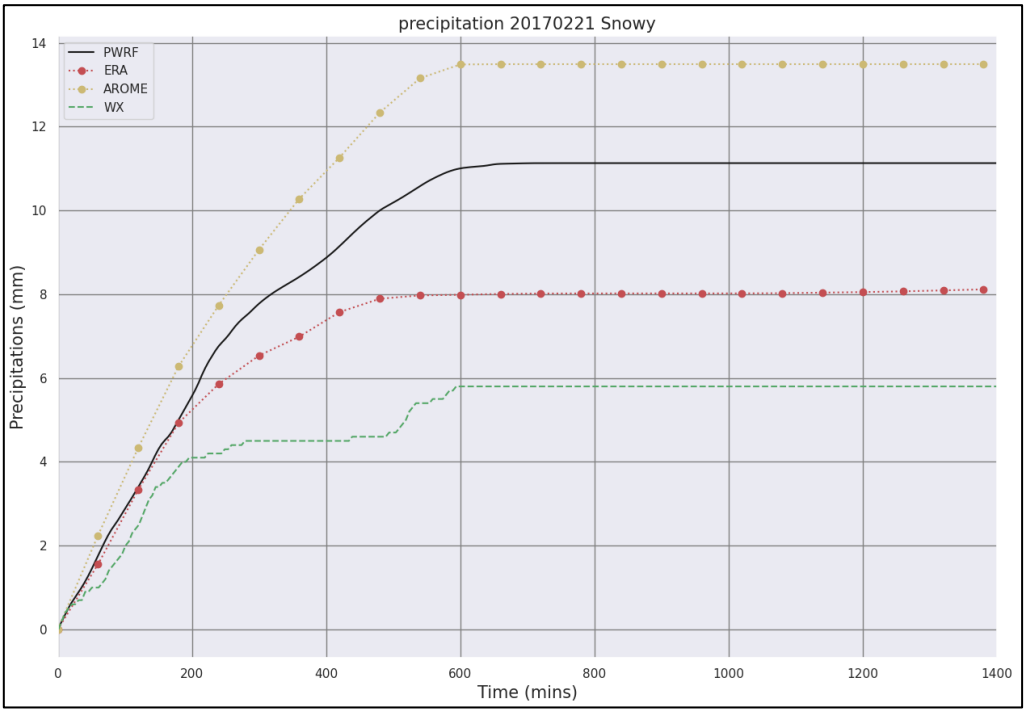

Figure 5 : Cumulative precipitation amount (water equivalent) on the SvalSat station on 02/21/2017, from PWRF simulations and from the various reference meteorological databases.

This result highlights the difficulties for PWRF to accurately reproduce precipitating events. It is however observed that the simulations (PWRF, AROME and ERA5) are in agreement with the measured data (THOR7) on the presence of a snow (precipitations et temperature below à 0) event occurring during the first 600 minutes of the day (00h-10h UTC) and followed by a calm afternoon.
The occurrence of mainly stratiform precipitation events (uniform over larger scales) in the region could explain the fairly good agreement between the ERA5 data and the other sources. The two simulations (PWRF and Arome-Arctic) seem to overestimate the total daily accumulated amount of precipitation compared to the WX rain gauge measurements, though freezing issues (see §3.4) may have cause some problems.

4.2 *Attenuations outputs*

The ability of the PWRF meteorological model coupled with the EMM module to reproduce the propagation channel behavior is presented in this section. In this study, the in-excess attenuation is considered as it can be easily obtained from the propagation experiment, without having to resort to a radiometer for the clear sky contribution. On the simulation side, the attenuations due to the hydrometeors only (cloud, rain, snow etc…) are considered in order to mimic a synthetic in-excess attenuation.

In the previous study [1], the results showed good correlations between the simulated attenuation time series and the experimental ones. Without a snow model, the ANS seemed capable of reproducing rainfall events, but proved unable to reproduce the CCDF (Complementary Cumulative Distribution Function) of in-excess attenuation. Although snow is not known to trigger strong attenuation events, we intend to see if the addition of a snow attenuation model makes it possible to fix this underestimation.

Figure 6.a shows the experimental (green) and synthetic (black) time series of in-excess attenuation. Because the experimental time series at 10 Hz is very noisy, it is first dowsample to 1Hz with a moving average. Then, a Butterworth low-pass filter (cuttof frequency=0.01 and sampling frequency fs=1) is used to remove the scintillation. To clarify the results a bit, we only display one point out of ten in the figure, but all the points are taken into account in figure 6.b. We clearly observe a concordance between the synthetic time series and the experimental one: the precipitation event is accounted for at the same time and with similar intensities, though the internal dynamics do not exactly match. Some of the differences could be explained by the different temporal sampling: a point every 5 min for the PWRF simulations and a point every second for the experimental data.
Figure 6.b represents the CCDF of in-excess attenuation derived from the PWRF synthetic time series and from the experimental. The statistics for the day are comparable even though the PWRF generates more attenuation. The probability of occurrence is higher with the experimental data because of the residual noise and scintillation encountered in the time series: noisy values below a few tenths of dB cannot be associated with actual in-excess attenuation. These statistics will have to be verified over longer study periods in order to really conclude on the capability of the model to produce reliable attenuation statistics.

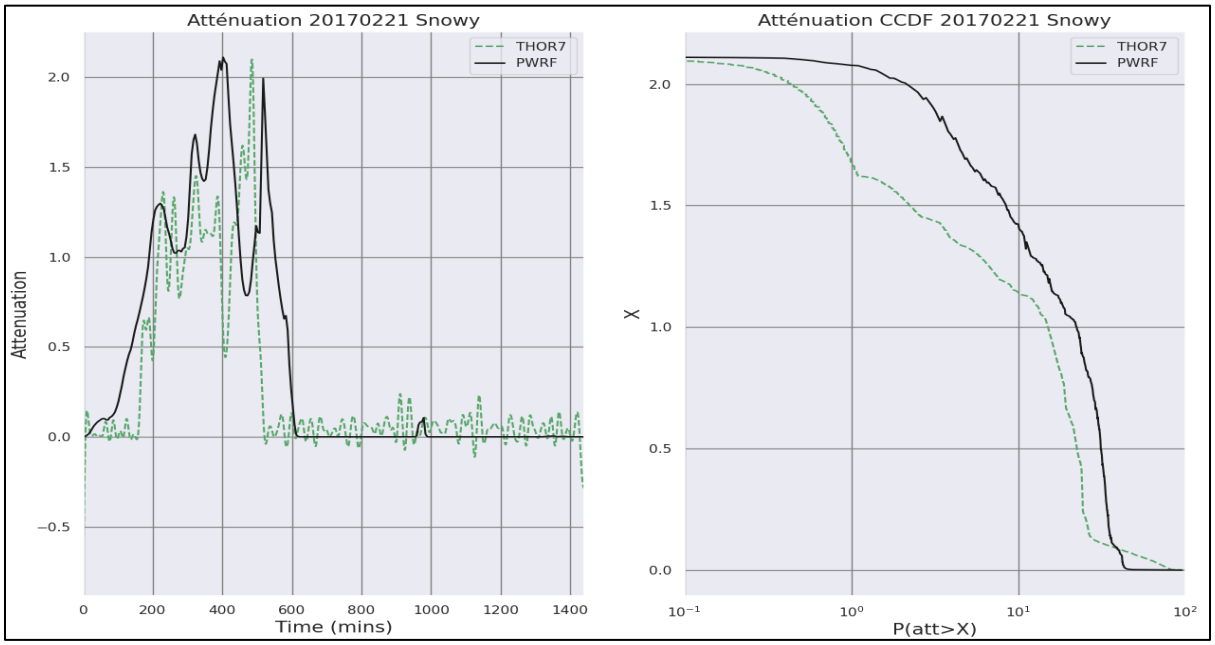

Figure 6 : Figure 6 : (a): In-excess attenuation time series (synthetic from PWRF simulations and experimental from THOR7 propagation measurements), SvalSat, 02-21-2017; (b) associated in-excess attenuation CCDF

5. Conclusions

In order to understand and quantify the effects of the polar meteorological conditions on microwave tropospheric propagation, the approach consisting in coupling a meteorological model with an EM module ([1],[2], [3]) is picked-up again and developed further with the introduction of a new multiphasic hydrometeor attenuation model. The WRF-ARW model previously used in [1] is traded for PWRF, a model specifically developed for high latitudes.

First, the meteorological simulations are compared to reference reanalysis dataset as well as meteorological measurements at the location of the THOR7 beacon receiver. The results for temperature and humidity are quite satisfactory. The simulations also seem to fairly well reproduce precipitation events despite some inconsistencies in precipitation intensity (accumulated precipitations at the end of the day).

Second, the simulated in-excess attenuation time series are compared to the experimental ones obtained from the THOR7 beacon. The ANS simulations present a good temporal/intensity agreement with the data as far as in-excess attenuation events are concerned. Although one day is a short period, comparing the attenuation statistics (CCDF) show good promise for the continuation of the study.

The next steps consists in selecting several representative days of polar climatology for further simulations, allowing to improve the parametrization of PWRF and of the snow attenuation model . In the end, the objective is to simulate the 2 years of the THOR7 propagation measurements with the best possible PWRF and EMM parametrization in order to obtain a good match between synthetic and measured statistics.

References

[1] Queyrel et al 2019. Preliminary Results of the THOR7 Propagation Experiment in the North Pole Region. Ka and Broadband Communications Conference.

[2] V. Le Mire, 2021, these: Modelling of Earth-space propagation in Ka-Band in tropical and equatorial regions.

[3] Fayon, G. 2017. Modelisation statistique de la diversité multi site aux fréquences comprises entre 20 et 50 GHz. PhD thèses, Université Toulouse 3 Paul Sabatier.

[4] Polar WRF team 2019. Polar WRF, Model Item, OpenGMS.

[5] W. C. Skamarock *et al.*, 2008, « A Description of the Advanced Research WRF Version 3. », NCAR, Boulder, CO, USA, Tech. Note NCAR/TN-475+STR.

[6] Zhang, C. and Y. Wang, 2017: Projected Future Changes of Tropical Cyclone Activity over the Western North and South Pacific in a 20-km-Mesh Regional Climate Model. *J. Climate*, 30, 5923-5941.

[7] H. Morrison & G.Thompson, 2009, Impact of Cloud Microphysics on the Development of Trailing Stratiform Precipitation in a Simulated Squall Line: Comparison of One- and Two-Moment Schemes. Monthly Weather Review, Vol 137, Issue 3.

[8] Sihvola, A. 2000, Mixing Rules with Complex Dielectric Coefficients. *Subsurface Sensing Technologies and Applications* 1, 393–415.

[9] Ray, P. S. 1972. Broadband complex refractive indices of ice and water. Appl. Opt., 11(8):1836?1844.

[10] Oguchi, T. 1983. Electromagnetic wave propagation and scattering in rain and other hydrometeors. Proceedings of the IEEE, 71(9):1029?1078.

[11] H. R. Pruppacher K. V. 1970, Beard, A wind tunnel investigation of the internal circulation and shape of water drops falling at terminal velocity in air Quarterly.

[12] Garrett, T. J., S. E. Yuter, C. Fallgatter, K. Shkurko, S. R. Rhodes, and J. L. Endries, 2015, Orientations and aspect ratios of falling snow. Geophys. Res. Lett., 42, 4617?4622, doi:10.1002/2015GL064040.

[13] ECMWF, IFS Documentation CY41R2, 2016, IFS Documentation.

[14] Seity, Y., P. Brousseau, S. Malardel, G. Hello, P. Bénard, F. Bouttier, C. Lac, and V. Masson, 2011: The AROME-France Convective-Scale Operational Model. Mon. Wea. Rev., 139, 976– 991.

[15] DMI/Xiohua Yang, 2020, Complete test and verification report on fully configured reanalysis and monitoring system.

[16] J. R. Houts, J. A. Nessel, and M. J. Zemba, *2016,* 'Design of a Ka-band propagation terminal for atmospheric measurements in polar regions', *10th European Conference on Antennas and Propagation (EuCAP)*, pp. 1–3.